Title
Particle size-controllable microwave-assisted solvothermal synthesis of the high-voltage cathode material LiCoPO4 using water/ethylene glycol solvent blends

Authors
Ludwig, Jennifer
Haering, Dominik
Doeff, Marca M
et al.

Publication Date
2017-03-01

DOI
10.1016/j.solidstatesciences.2017.01.009

Peer reviewed

Particle size-controllable microwave-assisted solvothermal synthesis of the high-voltage cathode material $LiCoPO_4$ using water/ethylene glycol solvent blends

Jennifer Ludwig [a], Dominik Haering [b], Marca M. Doeff [c], and Tom Nilges [a]*

[a] Technical University of Munich, Department of Chemistry, Synthesis and Characterization of Innovative Materials, Lichtenbergstr. 4, 85747 Garching, Germany

[b] Technical University of Munich, Department of Chemistry, Technical Electrochemistry, Lichtenbergstr. 4, 85747 Garching, Germany

[c] Lawrence Berkeley National Laboratory, Environmental Energy Technologies Division, 1 Cyclotron Rd, Berkeley, CA, 94720, USA

* Corresponding author. E-mail: tom.nilges@lrz.tum.de, Tel.: +49 89 289 13110, Fax: +49 89 289 13762

Abstract

Particle size-tuned platelets of the high-voltage cathode material $LiCoPO_4$ for Li-ion batteries have been synthesized by a simple one-step microwave-assisted solvothermal process using an array of water/ethylene glycol (EG) solvent mixtures. Particle size control was achieved by altering the concentration of the EG co-solvent in the mixture between 0 and 100 vol%, with amounts of 0–80 vol% EG producing single phase, olivine-type $LiCoPO_4$. The particle sizes of the olivine materials were significantly reduced from about 1.2 µm × 1.2 µm × 500 nm to 200 nm × 100 nm × 50 nm with increasing EG content, while specific surface areas increased from 2 to 13 $m^2 g^{-1}$. The size reduction could mainly be attributed to the modified viscosities of the solvent blends. Owing to the soft template effect of EG, the crystals exhibited the smallest dimensions along the [010] direction of the Li diffusion pathways in the olivine crystal structure, resulting in enhanced lithium diffusion properties. The relationship between the synthesis, crystal properties and electrochemical performance was further elucidated, indicating that the electrochemical performances of the as-prepared materials mainly depend on the solvent composition and the respective particle size range. $LiCoPO_4$ products obtained from reaction media with low and high EG contents exhibited good electrochemical performances (initial discharge capacities of 87–124 mAh g^{-1} at 0.1 C), whereas materials made from medium EG concentrations (40–60 vol% EG) showed the highest capacities and gravimetric energy densities (up to 137 mAh g^{-1} and 658 Wh kg^{-1} at 0.1 C), excellent rate capabilities, and cycle life.

Keywords

lithium cobalt phosphate; solvothermal synthesis; microwave synthesis; particle size control; high-voltage cathode; lithium-ion batteries

1 INTRODUCTION

A practical approach to increasing specific energies in Li-ion batteries would be to replace cathode materials that are currently used with those that operate at significantly higher redox potentials. The theoretical specific energy of the phospho-olivine $LiCoPO_4$ (LCP), which is redox active at ~4.8 V vs. Li^+/Li [1], is about 800 Wh kg^{-1}, compared to about 580 Wh kg^{-1} for the isostructural compound $LiFePO_4$ (LFP), which operates at ~3.45 V vs. Li^+/Li [2], and is used commercially in devices for applications such as plug-in hybrid electric vehicles [3]. Successful deployment of $LiCoPO_4$, however, has proven challenging due to its low and one-dimensional ([010] direction) electronic and ionic conductivities [4-6] and the limited oxidative stability of conventional electrolytic solutions [7]. Due to these issues, LCP materials frequently demonstrate poor electrochemical performance, including low capacities, low rate capabilities and capacity fading [8-11].

In addition to chemical doping [5, 6] and coating with conductive carbon [12, 13] to address the conductivity issues, synthetic methods that result in particle size reduction and good morphology control to improve the kinetics have been attempted [14]. The latter approach mainly involves kinetically controlled soft-chemical synthesis methods, including hydrothermal [15-17], solvothermal [18-21], sol-gel [22, 23], and polyol [24, 25] techniques. In solvothermal synthesis, for instance, the solvent composition has been shown to affect the particle size [26]. However, most of these processes are combined with high-temperature annealing and carbon coating to ensure good crystallinity and sufficient electronic conductivity [17, 18, 26].

We have recently reported [27] a facile, one-step microwave-assisted solvothermal (MWST) route to highly crystalline LCP, which requires no additional treatments such as high-temperature annealing or carbon coating. Under optimum conditions, hexagonal platelets with the smallest dimension along [010], the direction of Li diffusion in the olivine crystal structure [4, 6], are formed using a binary 1:1 (v:v) water/ethylene glycol (EG) solvent. The tuned crystal properties result in very good electrochemical performance (137 mAh g^{-1} at 0.1 C rate, using realistic active material loadings of 4–5 mg cm^{-2} in the composite electrodes). These promising results and the advantages of the microwave synthesis technique, which include extremely short reaction times and more uniform reaction conditions with lower temperature gradients resulting in monodisperse particles with controlled particle size range [27-32], prompted us to investigate this approach further to determine if we could further improve the electrochemical properties of LCP. In this work, we report the effect of the composition of binary water/ethylene glycol solvent mixtures on the structure, particle size and mor-

phology, and electrochemical performance of LCP materials made by microwave-assisted solvothermal synthesis.

2 EXPERIMENTAL

2.1 Microwave-assisted solvothermal synthesis

$LiCoPO_4$ powders were synthesized by a microwave-assisted solvothermal (MWST) process [27] using 0.944 g $LiOH \cdot H_2O$ (Bernd Kraft, ≥ 99.0%), 2.108 g $CoSO_4 \cdot 7\ H_2O$ (Chempur, 99%), and 0.865 g (0.506 mL) ortho-H_3PO_4 (AppliChem, Ph. Eur., 85 wt.% solution) in a molar ratio of Li:Co:P = 3:1:1, and 0.075 g ascorbic acid (Alfa Aesar, 99+%) as reducing agent to prevent oxidation of Co^{2+} to Co^{3+} in the aqueous solution. The two additional equivalents of Li are required to bind the SO_4^{2-} ions in the reaction. The reactants were dispersed in 30 mL of various water/ethylene glycol solvent mixtures (H_2O: Millipore water type I, 18.2 MΩ cm; EG: VWR AnalaR NORMAPUR, 99.9%). The EG concentration was varied in the range of 0–100 vol% with an increment step of 10 vol% while keeping all other parameters constant in order to ensure reliable and comparable results. In the following, the samples are designated LCP-0, LCP-10, (…), LCP-100, corresponding to the amount of EG in vol% (v:v) used in the solvent.

The resulting violet reaction mixtures (pH = 5.0) were homogenized and then transferred into 75 mL PTFE/TFM vessels (HTV-75, MLS GmbH). The synthesis was performed at 250 °C for 30 min using an Ethos One microwave system (MLS) equipped with an MR-8 HT high-temperature rotor. The system was operated at a maximum power of 600 W, and the microwave irradiation was adjusted automatically by the T660 temperature control unit. After the microwave treatment, the vessels were naturally cooled down. The pH of the solutions was 5.0–5.5. The products, which exhibited colors ranging from light pink to dark blue (detailed image see supplementary material, Fig. S1), were collected by filtration. The powders were washed several times with deionized water and absolute ethanol (VWR BDH PROLABO AnalaR NORMAPUR, 99.95%) and dried in air for 12 h at 150 °C.

2.2 Materials characterization

X-ray powder diffraction (PXRD) and Rietveld refinements. A Stoe STADI P diffractometer (Mo $K_{\alpha 1}$ radiation, λ = 0.70930 Å; Ge(111) monochromator; Dectris MYTHEN DCS 1K silicon solid-state detector) was used to collect PXRD data of the ground powders, which were sealed in 0.5 mm capillaries (Hilgenberg, borosilicate glass, wall thickness: 0.01 mm). The measurements were performed in a 2θ range of 3–60° (PSD step: 0.015°; time/step: 30 s, 3 ranges, measurement time: 12 h). The data were calibrated using an external Si standard (NBS, a = 5.43088 Å). Rietveld refinements of the diffraction patterns were performed with the Jana2006 software [33] using the olivine crystal structure model (space group *Pnma*, ICSD database entry no. 247497 [34]). In order to

ensure that the data were comparable, the same set of parameters was applied for all refinements. The background was fitted using a Chebyshev polynomial (35 coefficients). Peak asymmetry was corrected using the axial divergence model [35]. In addition, an absorption correction was applied (packing fraction: ~0.6). General atomic positions as well as the isotropic thermal displacement parameters of Co, P, and O were refined without restraints, whereas the parameters of Li were kept fixed due to its low atomic scattering factor. More realistic standard deviations were obtained by applying the Berar's correction [36].

Elemental analysis. Atomic absorption spectroscopy (Varian AA280FS sequential device) and photometry (Shimadzu UV-160 device) were used to analyze the Li, Co, and P contents. A Hekatech Euro EA CHNSO combustion analyzer was used to determine the C, H, N, and S contents.

Scanning electron microscopy (SEM). The morphology of the powders was examined by high-resolution scanning electron microscopy (HR-SEM) on a JEOL JSM-7500F instrument using an accelerating voltage of 1 kV, a LEI (lower electron secondary image) detector, and a working distance of 8 mm. The samples were prepared on conductive carbon tapes attached to an aluminum stub.

Transmission electron microscopy (TEM). A JEOL JEM-2010 transmission electron microscope (LaB_6 cathode, max. resolution: 0.2 nm) was used at 160 kV to perform selected area electron diffraction (SAED) experiments. Ethanolic dispersions of the powders were dried on 200 mesh carbon film for sample preparation.

BET Surface area analysis. The specific surface areas were measured by the Brunauer–Emmett–Teller (BET) method on a Quantachrome Autosorb iQ device using N_2 physisorption after a degassing period of 12 h at 423 K (11 measurement points).

Rheometry. The dynamic viscosities of the H_2O/EG solvent mixtures containing 0–100 vol% (v:v; increment step: 10 vol%) EG were measured at 25 °C using an MCR 302 Anton Paar Modular Compact Rheometer in parallel plate–plate geometry (PP-50 plate, diameter: 49.991 mm, gap: 0.250 mm). 10 mL of the solvent blends were prepared using a Brand Transferpette S (1–10 mL, error: ≤ ± 0.6%). A sample volume of ~0.5 mL was used for each measurement. Per solvent mixture, six measurements were performed in a shear rate range of 1–120 s^{-1} (40 measurement points, time/measurement: 10.2 s); the average viscosity was determined at a shear rate of 100 s^{-1}.

Electrochemical measurements. The electrochemical properties of electrodes made from the as-obtained LCP materials were tested using Swagelok cells with Li foil (Rockwood Lithium, 450 µm, battery grade, > 99.8%) as anode, two glass fiber separators (VWR, 691, 250 µm), and 80 µL electrolyte (1 M $LiPF_6$ in ethylene carbonate (EC)/dimethyl carbonate (DMC), 1:1 (w:w), Merck, LP30). The electrodes were prepared by mixing the LCP powders with conductive carbon (Super C65,

Timcal), polyvinylidene difluoride (PVdF, Kynar HSV 900, Arkema) and *N*-methyl-2-pyrrolidone (NMP, Sigma Aldrich) in a 80:10:10 wt% ratio followed by homogenization with a Thinky planetary centrifugal vacuum mixer (2000 rpm, 20 min). The mixture was spread on Al foil (15 µm, MTI) with a doctor-blade coater. Electrodes with a diameter of 10 mm and loadings of 4–5 mg cm^{-2} were cut out, pressed (KBr press, PerkinElmer) and dried for 2 h at 120 °C in a vacuum oven (Büchi B-585). The cells were assembled in a glove box (MBraun; Ar atmosphere, < 0.1 ppm H_2O, < 0.1 ppm O_2). Galvanostatic cycling was performed in a potential window of 3.5–5.2 V for three cycles each at 0.1 C, 0.2 C, 0.5 C, 1 C, and 2 C to test the C-rate capability, followed by 15 cycles at 0.5 C to evaluate the cycle life. The C rates were calculated from the theoretical capacity (167 mAh g^{-1}), neglecting a minor Li_2SO_4 impurity, which does not does not affect the electrochemical performance as shown in our previous work [27]. The potentiostatic step during CCCV (constant-current, constant-voltage) charging was limited to a current of 0.05 C. To ensure reproducibility, two cells per material were tested.

3 RESULTS AND DISCUSSION

3.1 X-ray powder diffraction

Fig. 1 shows the X-ray powder diffraction patterns of the samples LCP-0–LCP-80 prepared from the MWST process using concentrations of 0–80 vol% ethylene glycol in the binary solvent. The diffraction patterns can be fitted to the olivine crystal structure model (space group *Pnma*) [34] with overall excellent reliability factors (Fig. S2a–I), and no crystalline impurities were observed. The refined lattice parameters and cell volumes (Table S1) are comparable and in good agreement with reported values [27, 30, 37]. Considering the three sigma rule, there is evidence for a slight increase of the cell volume for samples made with higher EG concentrations. Although the narrow diffraction peaks suggest that all materials are highly crystalline as obtained from the MW synthesis without post-calcination, the increase of *V* with increasing amounts of EG in the solvent indicates that these products may have defects. The refinement of the occupancies, however, did not suggest Li-deficiencies or disordering, because of the limitations of the Rietveld method (*cf.* low atomic scattering factor of Li). Consequently, the occupancy factors of all sites were set to 1 and no site-mixing was assumed. Detailed crystal data (atomic coordinates, temperature factor, interatomic distances) are displayed in Tables S3 and S4.

Interestingly, the sample made with 90 vol% EG (LCP-90) contains a mixture of 87.4(4) wt% olivine LCP (*Pnma*) and 12.6(4) wt% of another, metastable LCP-polymorph ($Pna2_1$ [38]), while LCP-100 is pure $Pna2_1$-LCP (*cf.* Fig. S2j,k). The broad reflections are because the samples contain nanoparticles (*cf.* Fig. S4). The observation that at high EG contents, the metastable $Pna2_1$-modification is obtained, is consistent with another report [26] and indicates that the solvent significantly affects the phase formation during the solvothermal synthesis. A possible explanation is that diffusion plays a major role in the crystallization of the olivine phase during the process. In solvents with high EG contents, the viscosity and the boiling point of the mixture are increased (as discussed later), resulting in slower diffusion rates and reaction kinetics. Another possibility might be the decreased solubility of the precursors in solvent mixtures which contain less water [39]. Therefore, due to kinetic reaction control, the formation of metastable products ($Pna2_1$-LCP) is favored over thermodynamic products (*Pnma*-LCP). As the $Pna2_1$-LCP polymorph reportedly shows poor electrochemical performance [38, 40], this work will mainly focus on the electrochemically active, pure olivine materials LCP-0–80. A structure redetermination and thorough investigation of the formation and material properties of $Pna2_1$ based on LCP-100 is presented in another report [41].

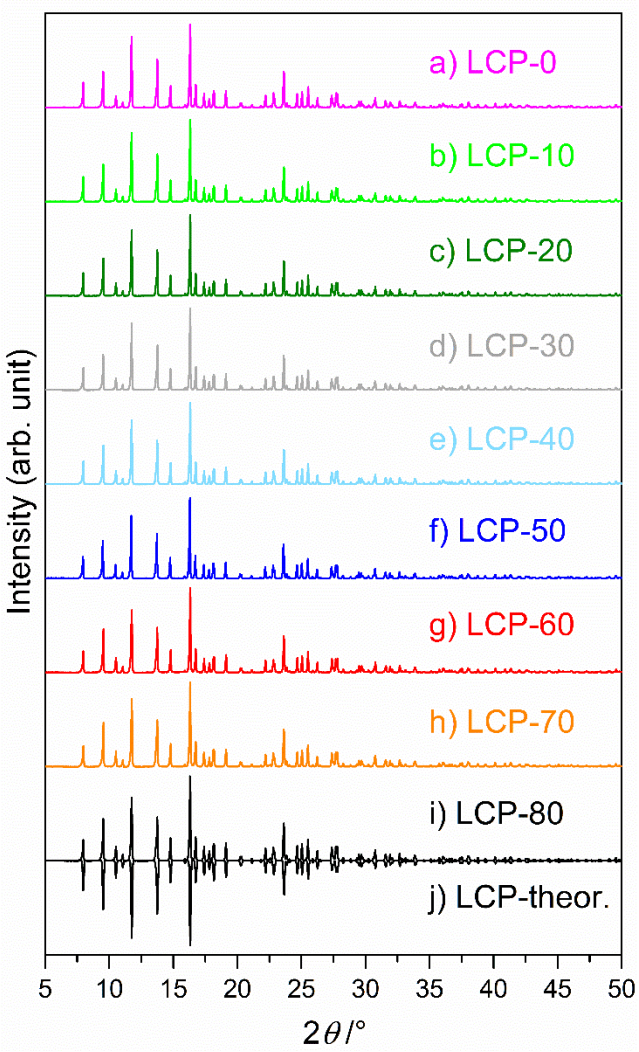

Fig. 1 X-ray powder diffraction patterns (Mo $K_{\alpha 1}$ radiation) of LCP powders obtained from MWST synthesis using various concentrations of EG (0–80 vol%) as co-solvent in a binary mixture with water: (a) LCP-0, (b) LCP-10, (c) LCP-20, (d) LCP-30, (e) LCP-40, (f) LCP-50, (g) LCP-60, (h) LCP-70, and (i) LCP-80. The theoretical pattern of LCP (*Pnma*) based on ICSD database entry no. 247497 [34] is displayed mirrored in (j).

3.2 Elemental analysis

The elemental compositions of the samples were analyzed by CHNS, AAS, and photometry. The results for LCP-0–80 are displayed in Table 2, for LCP-90 see Table S6 and reference [41] for LCP-100. While all the samples are slightly deficient both in Co and P compared to the theoretical values, with the deficit increasing as more EG was used in the synthesis, the Li content increases. The excess of Li is more evident when considering the molar ratios *n*(Li):*n*(P) and *n*(Co):*n*(P). Whilst the Co:P ratios are close to the expected ratio of 1:1 for all samples, the Li:P ratios range from 0.99(5):1

(LCP-0) to 1.22(5):1 (LCP-80). Taking the respective standard deviations into account, the observed rise in Li contents is significant.

Table 1 Elemental composition of the LCP samples synthesized by the MWST process using various concentrations of the co-solvent EG (0–80 vol%) in binary mixtures with water in comparison with the theoretical values [a,b]

Element	Theor.	LCP-0	LCP-10	LCP-20	LCP-30	LCP-40	LCP-50	LCP-60	LCP-70	LCP-80
S (wt%)	0	0.3(3)	0.5(3)	0.8(3)	0.9(3)	1.1(3)	1.4(3)	1.8(3)	2.1(3)	2.3(3)
Li (wt%)	4.3	4.1(2)	4.3(2)	4.4(2)	4.3(2)	4.3(2)	4.2(2)	4.6(2)	4.6(2)	4.8(2)
Co (wt%)	36.6	35.9(5)	35.6(5)	34.7(5)	34.8(5)	34.6(5)	34.1(5)	33.8(5)	33.4(5)	33.5(5)
P (wt%)	19.3	18.6(3)	18.5(3)	18.5(1)	18.2(3)	18.2(3)	17.9(3)	17.7(3)	17.5(3)	17.5(3)
n(Li):*n*(P)	1	0.99(5)	1.04(5)	1.06(5)	1.05(5)	1.05(5)	1.05(5)	1.16(5)	1.18(5)	1.22(5)
n(Co):*n*(P)	1	1.02(1)	1.01(1)	0.99(1)	1.00(1)	1.00(1)	1.00(1)	1.00(1)	1.01(1)	1.01(1)
Li_2SO_4 (wt %) [c]	0	0.9(10)	1.9(10)	2.8(10)	2.9(10)	3.9(10)	4.6(10)	6.2(10)	7.1(10)	7.9(10)
$LiCoPO_4$ (wt%) [d]	100	96.3(16)	96.1(16)	95.9(16)	94.5(16)	94.6(16)	92.8(16)	92.0(16)	90.6(16)	90.9(16)

[a] The composition is determined from the experimental results in wt% (standard deviations are given in parentheses).

[b] The values for C, H, and N were too low to be measured in all samples (= 0).

[c] Calculation based on the moles of S and the surplus of Li found.

[d] Calculation based on the moles of P found.

The variation of the Li contents can be explained by taking the CHNS analyses into consideration. Whilst no hydrogen and carbon are detected, which could be attributed to entrapped water or residues of the organic EG solvent and/or ascorbic acid reductive, substantial amounts of S are found, which increase linearly with higher vol% EG, similarly to the Li contents. As discussed in our previous work [27], the excess of Li and all of the detected S result from a minor Li_2SO_4 impurity, which is formed as an amorphous side product in the MWST reaction. The estimated Li_2SO_4 contents are found to be very low (*i.e.* not significant) for products obtained from water-rich solvents (*e.g.* 0.9 ± 1.0 wt% for LCP-0) and continuously increase (Fig. S3) to rather high fractions for products obtained from EG-rich media (*e.g.* 7.9 ± 1.0 wt% for LCP-80). This is also consistent with the observed Li:P molar ratios. An explanation for this is that Li_2SO_4 is a water soluble compound [42]. Therefore, when equal moles of $LiCoPO_4$ and Li_2SO_4 are formed in the reaction, the major portion of lithium sulfate is dissolved in the aqueous phase of the solvent. Residues on the surface of the particles are further removed by the washing step with water, while a minor fraction is found to form inclusions that

cannot be leached out [27]. With increasing EG concentrations and less water, the solubility of Li_2SO_4 in the solvent blend during the reaction is decreased. As a result, more Li_2SO_4 inclusions emerge in the particles upon crystallization. The fraction of the olivine active material is reduced to ~90 wt% for samples containing more Li_2SO_4 (*cf.* LCP-70,80).

3.3 Scanning electron microscopy

Fig. 2 shows the SEM images of the samples LCP-0–LCP-80 prepared using different amounts of EG in the solvent blend. The samples obtained from hydrothermal synthesis (0 vol% EG, LCP-0, Fig. 2a) and 10 vol% EG (LCP-10, Fig. 2b) exhibited irregular morphologies that vary from square platelets with a wide dimension range of about 0.5–1.2 µm × 0.5–1.2 µm and thicknesses of 150–500 nm to cubic shapes (~1 µm × 1 µm × 1 µm), some of the crystals being intergrown. Higher portions of EG (20–40 vol%), corresponding to the materials LCP-20, LCP-30, and LCP-40 (Fig. 2c–e), result in square platelets with edge lengths in the range of ~0.8–1.2 µm. With increasing EG concentration, the particle size distributions become more homogeneous and the base areas are marginally reduced. Moreover, the edges of the square base areas appear rounder (*cf.* LCP-40). The thickness of the platelets is reduced from about 150–500 nm (LCP-20) to a uniform 100 nm (LCP-40). Whereas a very small portion of 10 vol% EG has no significant impact on the particle size and morphology in comparison to the pure hydrothermal product LCP-0, moderate amounts up to 40 vol% EG help to prevent agglomeration and intergrowth of crystals, and reduce the thickness of the platelets. When the EG amount is raised to 50 vol% (LCP-50), corresponding to a 1:1 ratio (v:v), uniform hexagonal platelets of ~800–900 nm in length, 500–550 nm in width, and 130–180 nm in thickness (Fig. 2f) are produced as observed in our previous work [27]. At higher EG contents of 60–80 vol%, hexagonal platelets with overall smaller dimensions ranging from ~250–400 nm × 100–150 nm × 70 nm (LCP-60) to ~200–300 nm × 100–150 nm × 50–60 nm (LCP-80) and narrow particle size distributions were obtained (Fig. 2g–i). The overall size reduction with increasing EG concentration is in stark contrast to the fact that for LCP-20–40, primarily only the thickness was decreased. When comparing the hexagonal platelets to the ones obtained in 50 vol% EG, it is notable that the aspect ratio (length/width) of the base areas changes from approximately 1.6 (LCP-50) to about 2 (LCP-80). The particle size was further decreased for the non-olivine samples LCP-90 and LCP-100: LCP-90 exhibits two types of particles, nanospheres (diameter ~10–20 nm) located on the surface of hexagonal platelets (~300–600 nm × 80–150 nm × 30–60 nm; Fig. S4a–c), whereas LCP-100 only bears spherical particles (~15 nm; Fig. S4d–f).

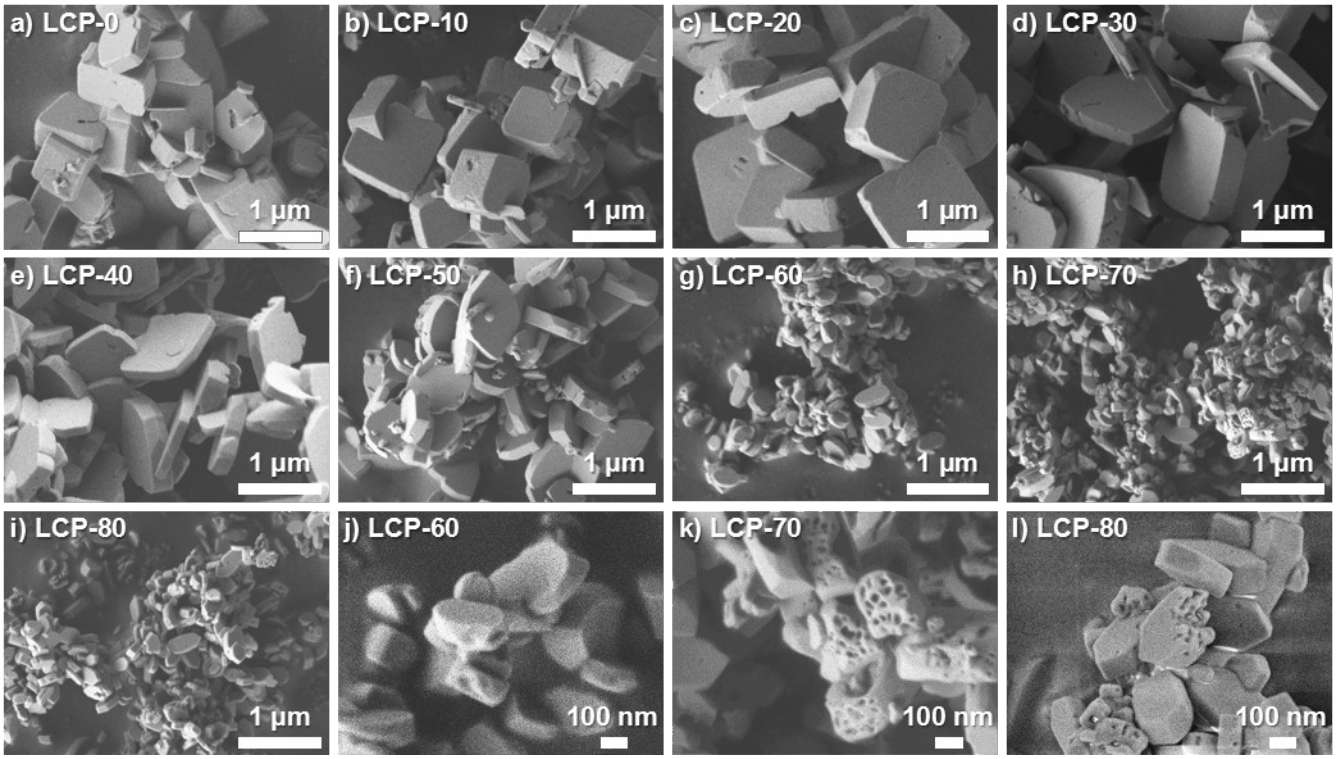

Fig. 2 SEM images of the LCP samples obtained from microwave-assisted solvothermal syntheses using various concentrations of EG (0–80 vol%) in binary H_2O/EG solvent blends: (a) LCP-0, (b) LCP-10, (c) LCP-20, (d) LCP-30, (e) LCP-40, (f) LCP-50, (g,j) LCP-60, (h,k) LCP-70, and (i,l) LCP-80.

Detailed images of broken crystals of LCP-60–80 at higher magnification (Fig. 2j–l) reveal that the hexagonal platelets exhibit an system of interconnected pores (diameter: ~10–20 nm), which are more prominent at higher EG concentrations and were also observed in our previous report [27]. The pores reduce the mechanical stability of the particles, which break upon stirring and during the washing step after the synthesis. In contrast, only very few pores and less fragmentation are observed for the bigger and mechanically more stable square platelets obtained from solvents containing more water (LCP-0–40). Here, the damage is more likely the result of the break-up of intergrown crystals. This finding is confirmed by TEM studies discussed later. The pores are the consequence of the formation mechanism, in which $LiCoPO_4$ and $Li_2SO_4 \cdot H_2O$ are obtained [27]. In mixtures with higher EG concentrations, the solubility of $Li_2SO_4 \cdot H_2O$ is decreased and a smaller amount dissolved. Hence, the composite crystals contain more Li_2SO_4 inclusions upon crystallization, which is in good agreement with the linearly increasing amounts of S found by CHNS analysis (*cf.* Table 2; Fig. S3). The pores observed on the breaking edges of fragmented particles (Fig. 2j–l) are due to the removal of the

inclusions upon washing. As the major portion of inclusions remains within the particles, the results of the elemental analysis are representative for the bulk materials.

The SEM studies reveal that primarily, the particle size and to a minor extent, the morphology of the crystals are affected by the solvent composition. The particle size and/or thickness is reduced at higher EG concentrations in the H_2O/EG solvent. At the same time, the morphology evolves from cubes and square platelets to hexagonal platelets.

3.4 BET surface area analysis

As expected from the SEM images, BET measurements deliver comparatively small specific surface areas for the materials LCP-0–80, which increase with increasing amounts of EG in the mixed H_2O/EG solvent (Fig. 3a). The samples LCP-0–LCP-30 show very similar small values of ~2–3 $m^2 g^{-1}$, indicating that the corresponding EG concentrations between 0 and 30 vol% have little effect on the particle size and thus, the surface area. For EG amounts between 40 vol% and 80 vol%, the surface areas are increased by a factor of two (LCP-40: ~4 $m^2 g^{-1}$) to six (LCP-80: ~13 $m^2 g^{-1}$) compared to the sample obtained from a pure water solvent (LCP-0: ~2 $m^2 g^{-1}$). Significantly higher surface areas could be obtained for the non-olivine materials LCP-90 (~22 $m^2 g^{-1}$) and LCP-100 (~61 $m^2 g^{-1}$). The correlation between BET surface areas and EG concentration is consistent with what has been observed previously for $LiMnPO_4$ [43].

Another interesting observation is that the colors of the powders (ranging from light pink for LCP-0 to dark blue for LCP-100; Fig. 3b), are related to the particle size and respective BET surface areas, as well as the structure. For the non-olivine samples LCP-90 and LCP-100, the blue color is caused by the presence of the metastable *Pna*2_1-polymorph of LCP, which exhibits a dark blue color [38].

Plotting the measured dynamic viscosities of the solvent mixtures, which are in good agreement with reported values [44, 45], versus the EG contents (Fig. 3c) reveals that the viscosities follow a similar exponential increase as the BET surface areas (Fig. 3a). Therefore, the increase in surface area and *vice versa* the decrease in particle size are highly correlated with the increasing viscosities of the solvents containing more of the EG co-solvent. An explanation for the key role of the EG concentration in tuning the particle size is that, because EG has a higher viscosity than water (EG: 15.7 ± 0.2 mPa·s *vs.* H_2O: 0.89 ± 0.05 mPa·s in our experiment at 25 °C), the ion diffusion rate in the solvent is reduced upon crystallization, which impedes the growth of large particles [39, 46]. Furthermore, the solubility of the precursors in the solvent is reduced compared to pure water [39], resulting in a higher degree of

supersaturation in EG-rich media. Hence, nucleation is favored over growth processes during crystal formation, resulting in smaller particles.

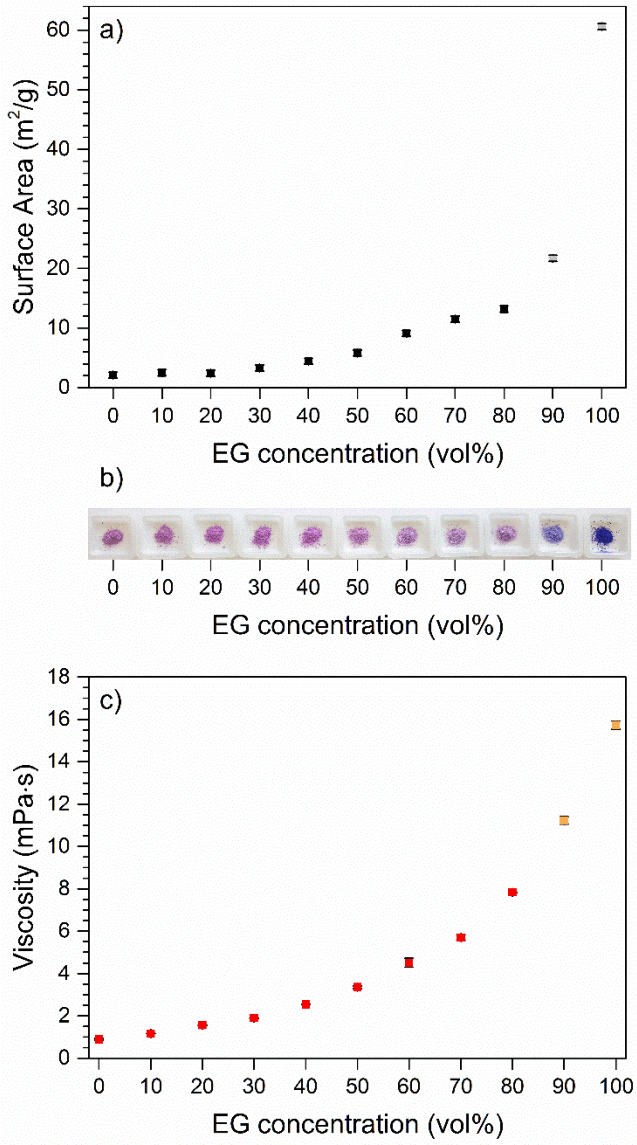

Fig. 3 (a) Specific surface areas of the LCP samples obtained from MWST synthesis versus the EG concentrations (0–100 vol%) used in the H_2O/EG solvent mixture, (b) color range of the as-obtained LCP powders, and (c) measured dynamic viscosities of the mixed solvents (average from six measurements, T = 25 °C, shear rate: 100 s^{-1}; error bars are smaller than data points where not visible). The data points of LCP-90 and LCP-100, which contain non-olivine LCP, are highlighted in different colors in (a,c).

However, it has to be noted that the viscosities were measured at ambient temperature and not the reaction temperature (250 °C), which is above the boiling points of the mixtures (*cf.* boiling point of pure EG: 198 °C [47]) [48]. Because the viscosity of the mixtures decreases with increasing temperature [45], and the particle size is more effectively regulated in mixtures that contain more EG, the size-regulating effect seems to play a major role in the precipitation step before the microwave-synthesis and the heat-up phase of the reaction, at which the solvents are still liquid. We therefore infer that the nucleation step is the most important with regard to controlling the crystal size by using binary aqueous solvents.

The solvent viscosity–BET area relation demonstrates that adjusting the viscosity of the solvent by varying the composition is a simple way to produce materials with tailored particle size using solvothermal synthesis, and also to predict the surface areas. The opportunity to modify this material property, which is crucial for the electrochemical performance of active materials, by a single synthesis parameter is of high interest for the commercial production of a variety of materials.

3.5 Transmission electron microscopy

The representative samples of the series LCP-0, LCP-30, LCP-50, and LCP-80 were further characterized by TEM (transmission electron microscopy) and SAED (selected area electron diffraction) to examine the crystal orientations and thicknesses as well as to gain further insights into the crystal formation and growth. To ensure that all crystals of a material are oriented identically, SAED patterns of 5–6 individual crystals were taken for each material. In addition, patterns of perpendicular crystal faces were collected. The respective TEM images and SAED patterns are presented in Fig. 4.

In general, the particle sizes and morphologies observed in the TEM images are in good agreement with the SEM studies. All the platelets are highly crystalline single crystals that are grown along the *ac* plane and show the smallest dimensions along the *b* axis, which is in the direction of the lithium diffusion pathways. Furthermore, the pore structures or Li_2SO_4 inclusions within the particles observed in the SEM (*cf.* Fig. 2i,k,l) are confirmed by the irregular transmission of the particles and are also more pronounced for higher EG contents (LCP-50 and LCP-80, Fig. 4i,m,o). The samples LCP-0 and LCP-30 consist of crystals with a square platelet morphology with the *a* and *c* axes being oriented along the diagonals of the base areas (Fig. 4a,e). The dimensions in the *ac* plane are similar (~1 µm × 1 µm), but the dimension along [010] is reduced from approximately 600 nm to 250 nm with the use of 30 vol% EG (Fig. 4c,g). In contrast, the hexagonal platelets of LCP-50 and LCP-80 show different dimensions in the base areas as well as the thicknesses. The particles of LCP-50 exhibit

dimensions of ~800 nm × 600 nm × 180 nm (Fig. 4i,k), while the platelets of LCP-80 are significantly smaller with a reduced size of ~300 nm × 150 nm × 50 nm (Fig. 4m,o). In both cases, the *c* axis is oriented along the longer side of the hexagonal base areas, the hexagonal shape of LCP-80 being elongated along [001].

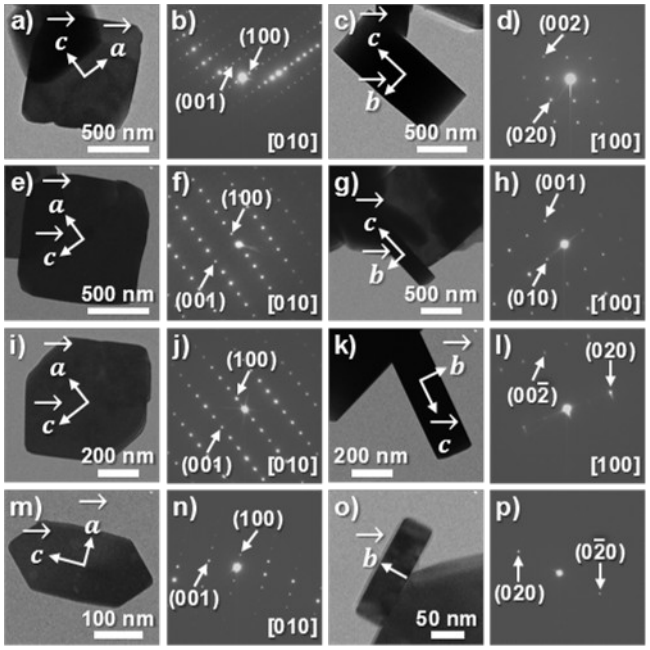

Fig. 4 TEM images and corresponding SAED patterns of the LCP samples synthesized by the MWST technique using various concentrations of EG (in vol%) as co-solvent in a mixture with water: (a–d) LCP-0, (e–h) LCP-30, (i–l) LCP-50, (m–p) LCP-80. Perpendicular crystal faces are displayed for each sample.

The TEM studies reveal that the EG co-solvent not only plays a key role in controlling the particle size by its higher viscosity compared to water (*cf.* Fig. 3). It also helps to promote the growth of crystals with defined morphology and orientation [43, 49]. An explanation for the anisotropic crystal properties is the soft template effect of the solvent [46]. EG molecules adsorb on the surface of the LCP nanocrystals by forming hydrogen-bonds between the hydroxyl groups and the oxygen atoms on the surface on the crystals, altering the surface energies of crystal faces. For $LiMnPO_4$, it was reported [43] that the EG molecules preferentially adsorb on the (100) planes, then the (010) planes, and the least favorable, the (001) planes, resulting in limited particle growth rates along the [100] and [010] directions compared to [001]. This is consistent with our observation that the platelets show a higher aspect ratio (*i.e.* elongation along *c*) for solvents containing more EG, but also with the reduction of the

particle thickness along [010] [43, 50]. Because Li-ion conduction in the olivine crystal structure is anisotropic, the reduced particle dimensions of our materials along [010] are expected to significantly enhance Li diffusion and thus, the electrochemical performance.

3.6 Electrochemical characterization

The olivine materials LCP-0–80 were tested in Swagelok half-cells without further processing (*e.g.*, annealing, carbon coating). The specific discharge capacities and respective coulombic efficiencies at different rates are displayed in Fig. 5. The corresponding galvanostatic curves can be found in Fig. S5. For better comparison of the trends in the test series, the first discharge capacity obtained at each C rate is displayed in Fig. 5a for the various cells. Generally, no obvious correlation of the performance with the particle size and thickness along [010] can be deduced. One would expect an increase in absolute capacities and C rate capabilities with decreasing [010] dimension due to shortened Li diffusion pathways, *i.e.*, the lowest value for LCP-0 (~600 nm, Fig. 4c) and the highest for LCP-80 (~50 nm, Fig. 4o). Instead, the following trends are observed at every C rate, with the capacity decreasing at higher rate (Fig. 5a): (1) LCP-0 and LCP-10 deliver low performances, (2) good to average performances are observed for LCP-20, LCP-30, LCP-60, LCP-70, and LCP-80, and (3) the best performance of the series is achieved for the samples LCP-40–60.

The relatively low capacities of LCP-0 and LCP-10 at both low (87 mAh g^{-1} and 116 mAh g^{-1} at 0.1 C) and higher rates can be explained by the large particle sizes (> 1 µm) and large dimensions along the [010] Li diffusion pathway (150–500 nm) as well as the inhomogeneous shapes (platelets, cubes) and particle sizes in both materials. However, the performance of the hydrothermal sample LCP-0 is still better than that of other hydrothermally synthesized $LiCoPO_4$ samples [17, 29], probably due to the improved crystallinity, which is the result of the microwave irradiation used for the synthesis [30]. The effect of decreasing the [010]-dimension from ~150–500 nm (LCP-20) to ~100 nm (LCP-40) is reflected in the increase in discharge capacity from 119 mAh g^{-1} to 137 mAh g^{-1} at 0.1 C. Moreover, these materials show more uniform particle sizes and morphologies compared to LCP-0 and LCP-10. The highest capacities at every rate and best coulombic efficiencies are achieved for the hexagonal platelets of LCP-50. The value of 136 mAh g^{-1} at 0.1 C corresponds to a gravimetric energy density of 653 Wh kg^{-1} (based on its capacity and discharge potential of 4.8 V). LCP-40 reaches a capacity of 137 mAh g^{-1} at 0.1 C (energy density of 658 Wh kg^{-1}), but exhibits a lower rate capability. Both results are among the best results for LCP so far [21, 26, 30, 32], and comparable to our previous work [27]. This is surprising as the particles exhibit bigger dimensions (~130–180 nm) in the [010] Li diffusion

direction compared to LCP-60–80 (~50–70 nm). Unexpectedly, these samples with the smallest and most homogeneous particles as well as the smallest dimension along [010] are not the best performing of the series, suggesting that there is no linear correlation with the particle size or [010] dimension, which is reflected by the somewhat lower initial discharge capacities (122–131 mAh g^{-1} at 0.1 C) and C rate capabilities. Because LCP is electrochemically active above 4.6 V, side reactions involving the oxidation of

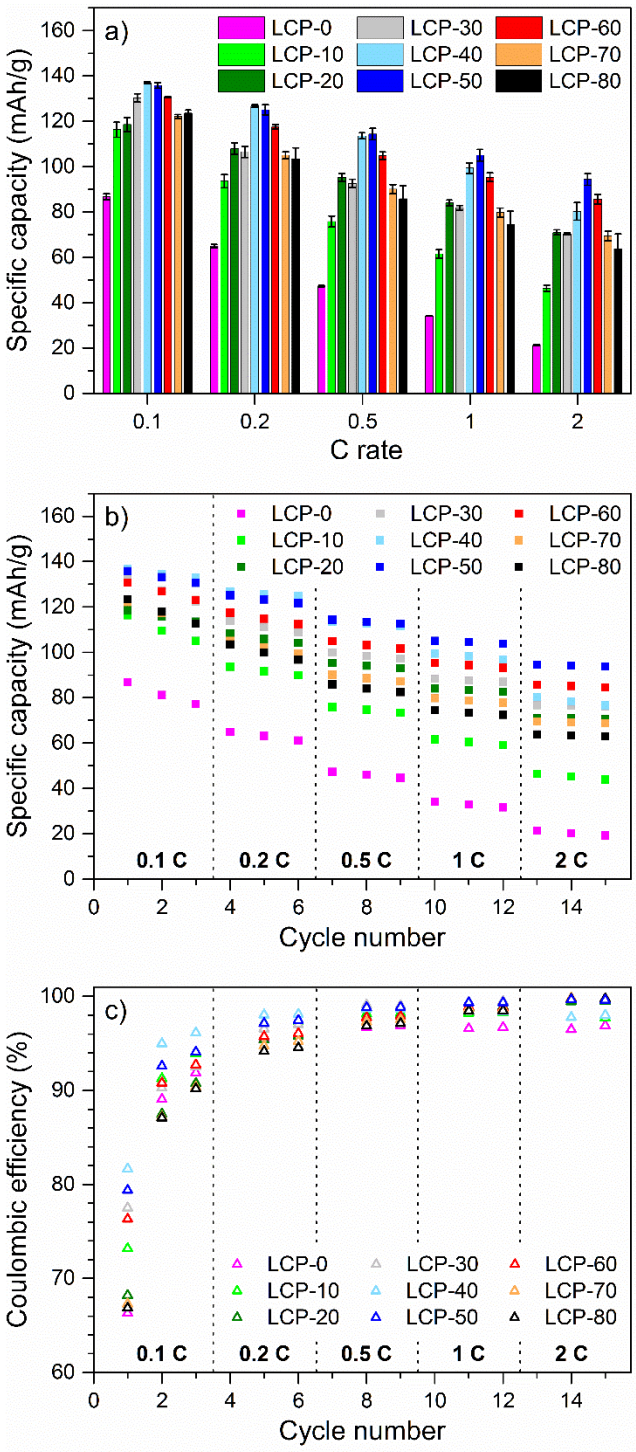

Fig. 5 (a) Specific discharge capacities *vs.* C rate for the 1st cycle of each C rate (error bars represent standard deviations from two cells), (b) specific discharge capacities *vs.* C rate for the first three cycles at each C rate, and (c) coulombic efficiencies for the LCP samples made by the MWST process using various amounts of EG (0–80 vol%) The efficiencies of the 1st cycle after each C rate increase are omitted in (c) as they cannot be determined in these cases. All data points present the average values from two cells. Data points which are not visible are overlapped by other symbols. The error bars in (b,c) are omitted for clarity. Conditions: 1 M $LiPF_6$ in EC:DMC (1:1, w:w) at 25 °C.

the electrolyte [7] compete with the (de)intercalation reaction of LCP. The high specific surface areas of the materials LCP-60–80 (~9–13 $m^2 g^{-1}$ *vs.* ~4–6 $m^2 g^{-1}$ for LCP-40 and LCP-50) exacerbate these side reactions, resulting in poorer performance and lower coulombic efficiencies. The decomposition products of the side reactions are likely to form resistive films on the particle surface that impede lithium diffusion [51]. This finding strongly contrasts the general assumption [13, 52] that particle size reduction helps to improve the electrochemical performance. Consequently, due to side reactions, the particle size reduction is not necessarily beneficial to performance, particularly for high voltage materials.

Following the C rate test, the cycle life of the LCP electrodes was tested for 15 cycles at a 0.5 C discharge rate (Fig. 6). The total capacities (Fig. 6a), capacity retentions, and coulombic efficiencies (Fig. 6b) follow the same trends as observed in the rate capability tests at higher C rates (*cf.* Fig. 5a,b, cycles 10–15), with the minimum being reached for LCP-0, and the maximum for LCP-40 and LCP-50. Despite the variation in capacity, the samples LCP-20–80 show an excellent electrochemical stability, which is among the best performances reported as LCP materials have been shown to suffer from poor cycling stability [7, 10]. The cycle life of the best-performing materials in terms of absolute capacity, LCP-40 and LCP-50, however, differs greatly. While LCP-50 with a specific capacity of 101 mAh g^{-1} maintains 94% of its original value in the 15^{th} cycle, LCP-40 shows rapid fading and only reaches a capacity of 73 mAh g^{-1} (79%), which is only the fourth best value of the sample series. The deviant cycle life may be the consequence of different particle size ranges, thicknesses along [010], and crystal shapes. The influence of the shape is further supported by the fact that capacity fading is faster for samples with a square platelet morphology (LCP-0–40) than for materials that contain hexagonal shapes (LCP-50–80).

Also note that the performances cannot be directly correlated with the contents of the Li_2SO_4 side phase, which rise linearly with increasing EG concentration used for the synthesis (*cf.* Table 2 and Fig. S3). This is in line with our previous results [27], which suggested that the impurity does not affect the electrochemical performance.

In brief, the electrochemical performance is the result of superimposed effects such as crystallite size, particle shape, and thickness in the [010] direction of the Li diffusion pathways. Consequently, a straightforward explanation for the observed trends cannot be deduced from our current findings. The results, however, indicate that with the exception of LCP-0 and LCP-10, all the samples synthesized in solvents with medium EG contents and respective medium particle sizes show above-average to excellent discharge capacities, rate capabilities and cycle life, the optimum being reached at 50 vol% EG. In comparison to previous reports of poor cycling stability for LCP [8-11], the cycle life was

significantly improved. This suggests that in contrast to cathode materials with lower operating voltage like LFP (3.45 V [2]) [53, 54], a medium particle size range seems to be beneficial for high-voltage cathode materials such as LCP. This finding is consistent with other studies conducted by our group [55] as well as with reports about other high-voltage cathode materials [56-58].

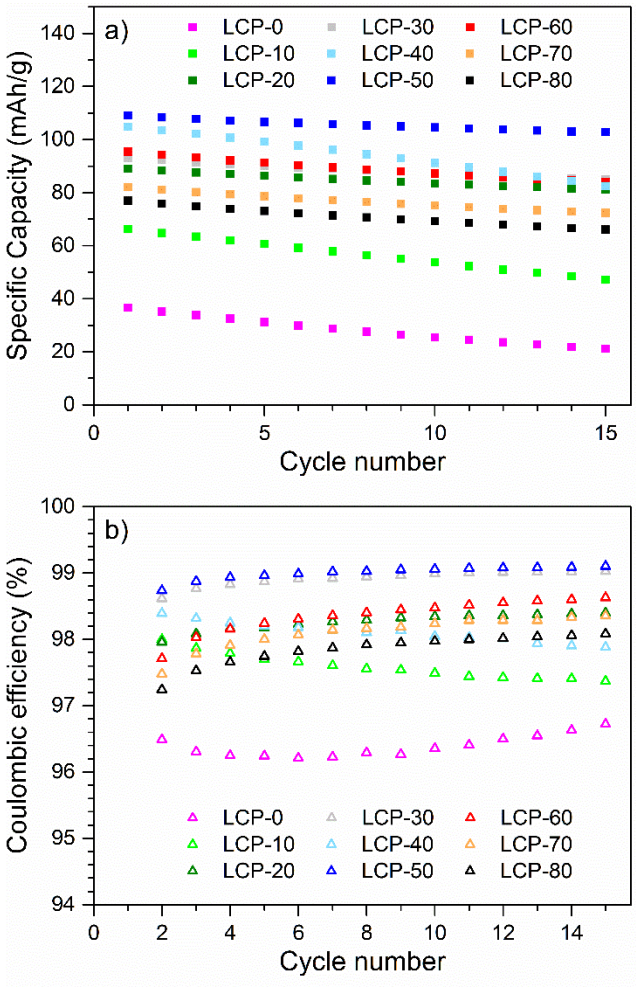

Fig. 6 Comparison of the (a) electrochemical stabilities (average values from two cells, error bars are omitted for clarity) and (b) coulombic efficiencies of the LCP samples prepared by MWST syntheses using various amounts of EG (0–80 vol%) at 0.5 C after the first 15 cycles of C rate testing. The coulombic efficiencies of the 1st cycle are not shown as they cannot be determined due to the C rate change before the cycle life test. Conditions: 1 M $LiPF_6$ in EC:DMC (1:1, w:w) at 25 °C.

4 CONCLUSIONS

Particle size-controlled powders of the high-voltage cathode material $LiCoPO_4$ with platelet-like morphologies have been synthesized *via* a rapid one-step microwave-assisted solvothermal route at moderate temperatures using a variety of water/ethylene glycol (EG) mixed solvents. Particle size control was demonstrated by varying the concentration of the EG co-solvent in the solvent mixture between 0–100 vol% with an increment step of 10 vol%.

X-ray powder diffraction experiments reveal that highly crystalline, olivine-type LCP (space group *Pnma*) is obtained for EG contents between 0–80 vol%. At higher EG concentrations, the formation of a metastable LCP polymorph ($Pna2_1$) was observed. SEM studies indicate that, whereas at low EG amounts (0–40 vol%), the formation of square platelets or cubic crystals with inhomogeneous particle size distributions is preferred, uniform hexagonal platelets are formed in solvent mixtures with 50–80 vol% EG. Owing to the higher viscosity of the reaction medium with increasing EG concentrations, the particle dimensions are significantly reduced from approximately 1.2 µm × 1.2 µm × 500 nm to 200 nm × 100 nm × 50 nm in EG-rich mixtures, which is consistent with an increase in BET surface areas. According to TEM studies, EG not only exhibits a size-regulating effect, but is also a soft template which promotes the crystal growth by selective adsorption on crystal faces. As a result, all particles show the reduced dimensions along the [010] direction of the Li diffusion pathways in the crystal structure, which is beneficial to enhance the Li-ion diffusivity and thus improve the electrochemical performance.

The performance of the as-prepared LCP materials strongly depends on the solvent composition, and the respective size range and thickness of the platelets. LCP made from mixtures with low and high EG contents exhibit average specific capacities and rate capabilities, which is the result of big and inhomogeneous crystallite sizes, and increased side reactions of powders with high specific surface areas with the electrolyte at high voltage. The materials synthesized in medium EG concentrations of 40–60 vol%, on the other hand, show the highest initial discharge capacities of up to 137 mAh g^{-1} at 0.1 C, excellent rate performance, and cycle life although the materials did not undergo further treatment (annealing, coating). Our findings suggest that in contrast to cathode materials with lower operating voltage (*e.g.* LFP), a medium particle size range is the optimum for high-voltage materials such as LCP.

To conclude, the present work not only provides a simple and efficient, but also energy- and cost-saving approach towards particle size control of cathode materials by microwave-assisted synthesis. It was also shown that the electrochemical performance can be improved by simply adjusting

one synthesis parameter such as the solvent composition and respective viscosity, which might be of interest for large-scale industrial manufacturing. Therefore, the influence of the solvent mixing ratio on the material properties should also be investigated for alternative co-solvents with morphology-tuning properties, such as polyols (*e.g.* diethylene glycol, triethylene glycol, tetraethylene glycol, polyethylene glycol).

Abbreviations

AAS	Atomic absorption spectroscopy
BET	Brunauer–Emmett–Teller
CCCV	Constant-current, constant-voltage
DMC	Dimethyl carbonate
EC	Ethylene carbonate
EG	Ethylene glycol
HR	High-resolution
LCP	Lithium cobalt phosphate, $LiCoPO_4$
LEI	Lower electron secondary image
LFP	Lithium iron phosphate, $LiFePO_4$
MWST	Microwave-assisted solvothermal
NMP	*N*-Methyl-2-pyrrolidone
PVdF	Polyvinylidene difluoride
PXRD	X-ray powder diffraction
SAED	Selected area electron diffraction
SEM	Scanning electron microscope
TEM	Transmission electron microscopy

Author contributions

J. L. and T. N. conceived and designed this work, and J. L. carried out the synthetic experiments and material characterization. D. H. performed the BET measurements and electrochemical tests. J. L. wrote the publication. All authors participated in discussion of the results and this manuscript.

Acknowledgements

The authors would like to thank BMW for financial support. We also thank C. Stinner and H. Gasteiger for their participation in the discussion of the results. The help of U. Ammari with elemental analyses,

K. Rodewald with SEM, and M. Hanzlik with TEM measurements is gratefully acknowledged. Special thanks go to C. Marino for the help with the electrochemical measurements and for proofreading this manuscript. J. Ludwig is further grateful to the Fonds der Chemischen Industrie for her PhD fellowship.

Supplementary material

Supplementary material related to this article: Colors of LCP-0–100, Rietveld fits and crystallographic data of LCP-0–100; elemental analysis of LCP-90; S and Li_2SO_4 contents versus EG concentration; SEM images of LCP-90 and LCP-100; galvanostatic curves of LCP-0–LCP-80 in the first three cycles at various C rates. This material can be found at http://dx.doi.org/10.1016/j.solidstatesciences.xxxx.xx.xxx. The crystallographic data for this paper in CIF format can be found in CSD xxx–xxx.

References

[1] K. Amine, H. Yasuda, M. Yamachi, Electrochem. Solid-State Lett., 3 (2000) 178-179.

[2] A.K. Padhi, K.S. Nanjundaswamy, J.B. Goodenough, J. Electrochem. Soc., 144 (1997) 1188-1194.

[3] W.-J. Zhang, J. Power Sources, 196 (2011) 2962-2970.

[4] D. Morgan, A. Van der Ven, G. Ceder, Electrochem. Solid-State Lett., 7 (2003) A30-A32.

[5] J. Wolfenstine, J. Power Sources, 158 (2006) 1431-1435.

[6] C.A.J. Fisher, P.V.M. Hart, M.S. Islam, Chem. Mater., 20 (2008) 5907-5915.

[7] M. Egashira, H. Takahashi, S. Okada, J.-I. Yamaki, J. Power Sources, 92 (2001) 267-271.

[8] S. Okada, S. Sawa, M. Egashira, J. Yamaki, M. Tabuchi, H. Kageyama, T. Konishi, A. Yoshino, J. Power Sources, 97-98 (2001) 430-432.

[9] N.N. Bramnik, K. Nikolowski, C. Baehtz, K.G. Bramnik, H. Ehrenberg, Chem. Mater., 19 (2007) 908-915.

[10] E. Markevich, R. Sharabi, H. Gottlieb, V. Borgel, K. Fridman, G. Salitra, D. Aurbach, G. Semrau, M.A. Schmidt, N. Schall, C. Bruenig, Electrochem. Commun., 15 (2012) 22-25.

[11] K. Zaghib, A. Guerfi, P. Hovington, A. Vijh, M. Trudeau, A. Mauger, J.B. Goodenough, C.M. Julien, J. Power Sources, 232 (2013) 357-369.

[12] J. Wolfenstine, J. Read, J.L. Allen, J. Power Sources, 163 (2007) 1070-1073.

[13] J. Liu, T.E. Conry, X. Song, L. Yang, M.M. Doeff, T.J. Richardson, J. Mater. Chem., 21 (2011) 9984-9987.

[14] S. Brutti, P. Reale, E. Piciollo, V. Gentili, P.G. Bruce, B. Scrosati, S. Panero, Prepr. Symp. - Am. Chem. Soc., Div. Fuel Chem., 57 (2012) 737-739.
[15] X. Huang, J. Ma, P. Wu, Y. Hu, J. Dai, Z. Zhu, H. Chen, H. Wang, Mater. Lett., 59 (2005) 578-582.
[16] J. Chen, M.J. Vacchio, S. Wang, N. Chernova, P.Y. Zavalij, M.S. Whittingham, Solid State Ionics, 178 (2008) 1676-1693.
[17] M. Kotobuki, Y. Mizuno, H. Munakata, K. Kanamura, Phosphorus Res. Bull., 24 (2010) 12-15.
[18] F. Wang, J. Yang, Y. Nuli, J. Wang, J. Power Sources, 196 (2011) 4806-4810.
[19] J. Su, B.-Q. Wei, J.-P. Rong, W.-Y. Yin, Z.-X. Ye, X.-Q. Tian, L. Ren, M.-H. Cao, C.-W. Hu, J. Solid State Chem., 184 (2011) 2909-2919.
[20] X. Rui, X. Zhao, Z. Lu, H. Tan, D. Sim, H.H. Hng, R. Yazami, T.M. Lim, Q. Yan, ACS Nano, 7 (2013) 5637-5646.
[21] S. Brutti, J. Manzi, A. De Bonis, D. Di Lecce, F. Vitucci, A. Paolone, F. Trequattrini, S. Panero, Mater. Lett., 145 (2015) 324-327.
[22] Gangulibabu, D. Bhuvaneswari, N. Kalaiselvi, N. Jayaprakash, P. Periasamy, J. Sol-Gel Sci. Technol., 49 (2009) 137-144.
[23] M.S. Bhuwaneswari, L. Dimesso, W. Jaegermann, J. Sol-Gel Sci. Technol., 56 (2010) 320-326.
[24] P.R. Kumar, M. Venkateswarlu, M. Misra, A.K. Mohanty, N. Satyanayana, J. Nanosci. Nanotechnol., 11 (2011) 3314-3322.
[25] N. Padmanathan, S. Selladurai, Asian J. Chem., 25 (2013) 9605-9609.
[26] B. Wu, H. Xu, D. Mu, L. Shi, B. Jiang, L. Gai, L. Wang, Q. Liu, L. Ben, F. Wu, J. Power Sources, 304 (2016) 181-188.
[27] J. Ludwig, C. Marino, D. Haering, C. Stinner, D. Nordlund, M.M. Doeff, H.A. Gasteiger, T. Nilges, RSC Adv., 6 (2016) 82984-82994.
[28] J.A. Gerbec, D. Magana, A. Washington, G.F. Strouse, J. Am. Chem. Soc., 127 (2005) 15791-15800.
[29] A.V. Murugan, T. Muraliganth, A. Manthiram, J. Electrochem. Soc., 156 (2009) A79-A83.
[30] A.V. Murugan, T. Muraliganth, P.J. Ferreira, A. Manthiram, Inorg. Chem., 48 (2009) 946-952.
[31] I. Bilecka, M. Niederberger, Nanoscale, 2 (2010) 1358-1374.
[32] R.E. Rogers, G.M. Clarke, O.N. Matthew, M.J. Ganter, R.A. DiLeo, J.W. Staub, M.W. Forney, B.J. Landi, J. Appl. Electrochem., 43 (2013) 271-278.
[33] V. Petricek, M. Dusek, L. Palatinus, Z. Kristallogr. - Cryst. Mater., 229 (2014) 345-352.
[34] V. Koleva, E. Zhecheva, R. Stoyanova, Eur. J. Inorg. Chem., (2010) 4091-4099.
[35] L.W. Finger, D.E. Cox, A.P. Jephcoat, J. Appl. Crystallogr., 27 (1994) 892-900.

[36] J.F. Berar, P. Lelann, J. Appl. Crystallogr., 24 (1991) 1-5.
[37] J. Chen, S. Wang, M.S. Whittingham, J. Power Sources, 174 (2007) 442-448.
[38] C. Jaehne, C. Neef, C. Koo, H.-P. Meyer, R. Klingeler, J. Mater. Chem. A, 1 (2013) 2856-2862.
[39] F. Teng, S. Santhanagopalan, A. Asthana, X.-B. Geng, S.-I. Mho, R. Shahbazian-Yassar, D.D.-S. Meng, J. Cryst. Growth, 312 (2010) 3493-3502.
[40] K.J. Kreder, G. Assat, A. Manthiram, Chem. Mater., 27 (2015) 5543-5549.
[41] J. Ludwig, D. Nordlund, M.M. Doeff, T. Nilges, xxx, submitted, (2016).
[42] W.F. Linke, A. Seidell, Solubilities of In-organic and Metal Organic Compounds Vol. II. 4th ed, Am. Chem. Soc., 1966.
[43] Y. Hong, Z. Tang, S. Wang, W. Quan, Z. Zhang, J. Mater. Chem. A, 3 (2015) 10267-10274.
[44] N.G. Tsierkezos, I.E. Molinou, J. Chem. Eng. Data, 43 (1998) 989-993.
[45] T. Sun, A.S. Teja, J. Chem. Eng. Data, 48 (2003) 198-202.
[46] S. Kuppan, P. Balaya, M.V. Reddy, B.V.R. Chowdari, J.J. Vittal, Energy Environ. Sci., 3 (2010) 457-464.
[47] S. Rebsdat, D. Mayer, Ethylene Glycol, in: Ullmann's Encyclopedia of Industrial Chemistry, Wiley-VCH 2000, pp. 531-546.
[48] H.M. Trimble, W. Potts, Ind. Eng. Chem., 27 (1935) 66-68.
[49] X. Qin, J. Wang, J. Xie, F. Li, L. Wen, X. Wang, Phys. Chem. Chem. Phys., 14 (2012) 2669-2677.
[50] M. Wu, Z.H. Wang, L.X. Yuan, W.X. Zhang, X.L. Hu, Y.H. Huang, Chin. Sci. Bull., 57 (2012) 4170-4175.
[51] D. Aurbach, B. Markovsky, G. Salitra, E. Markevich, Y. Talyossef, M. Koltypin, L. Nazar, B. Ellis, D. Kovacheva, J. Power Sources, 165 (2007) 491-499.
[52] T.N.L. Doan, I. Taniguchi, J. Power Sources, 196 (2011) 5679-5684.
[53] C. Delacourt, P. Poizot, S. Levasseur, C. Masquelier, Electrochem. Solid-State Lett., 9 (2006) A352-A355.
[54] M. Gaberscek, R. Dominko, J. Jamnik, Electrochem. Commun., 9 (2007) 2778-2783.
[55] J. Ludwig, C. Marino, D. Haering, C. Stinner, H.A. Gasteiger, T. Nilges, J. Mater. Chem. A, (2016) submitted.
[56] S.K. Martha, H. Sclar, Z. Szmuk Framowitz, D. Kovacheva, N. Saliyski, Y. Gofer, P. Sharon, E. Golik, B. Markovsky, D. Aurbach, J. Power Sources, 189 (2009) 248-255.
[57] K.C. Karn, M.M. Doeff, Mater. Matters (Milwaukee, WI, U. S.), 7 (2012) 56-60.
[58] L. Xiao, Y. Guo, D. Qu, B. Deng, H. Liu, D. Tang, J. Power Sources, 225 (2013) 286-292.